ISBN: 978-3-95450-132-8 doi:10.18429/JACoW-IPAC2014-THPRO086

FLAT-BEAM GENERATION AND COMPRESSION AT THE FERMILAB'S ADVANCED SUPERCONDUCTING TEST ACCELERATOR*

J. Zhu[a,b,#], P. Piot[a,c], D. Mihalcea[c], C. R. Prokop[c]
[a]Fermilab, Batavia, IL 60510, USA
[b]IFP, CAEP, Mianyang 621900, China
[c]NIU, DeKalb, IL 60115, USA

Abstract

An important asset of Fermilab's Advanced Superconducting Test Accelerator (ASTA) is its ability to generate flat beams with high-transverse emittance ratios. In this paper, we present a practical design and simulation of flat beam generation and compression with various bunch charges up to 3.2 nC. Emittance growth within the round-to-flat beam transformer and the impact of low energy compression is discussed in detail. Finally, it is found that the compressed flat beam could provide exciting opportunities in the field of advanced acceleration techniques and accelerator-based light source.

INTRODUCTION

Flat beams with high-emittance ratio directly generated in a photoinjector via round-to-flat beam transformation (RFBT) of angular-momentum-dominated beams have many attracting applications [1-4]. During this process, the canonical angular momentum (CAM) of the beam is removed using a RFBT insertion consisting of three skew quadrupole magnets. The CAM-dominated beam is transformed into a flat beam with transverse geometric emittances [5]:

$$\varepsilon_{\pm} = \sqrt{\varepsilon_u^2 + 1^2} \pm 1 \xrightarrow{1 ? \varepsilon_u} \left\{ \varepsilon_+ \approx 2l \qquad \varepsilon_- \approx \varepsilon_u^2 / 2l \right\}, \quad (1)$$

where ε_u is the uncorrelated geometric emittance, $l = \langle L \rangle / 2p_z$ with $\langle L \rangle$ the CAM introduced at the surface of the cathode and p_z is the longitudinal momentum. The emittances of the flat beam coincide with the eigen-emittances [6] of the CAM-dominated beam $\varepsilon_{\pm}=\varepsilon_{\text{eigen},\pm}$.

This flat-beam source has been experimentally demonstrated at the Fermilab A0 Photoinjector Laboratory (A0PI) [7], where an emittance ratio of ~100 was achieved for a bunch charge of ~0.5 nC with the smaller emittance of the flat beam of ~0.41 μm.

FLAT-BEAM GENERATION AT ASTA

The ASTA photoinjector is diagrammed in Fig. 1. A series of simulations were performed with ASTRA [8] to optimize the ASTA injector setups to produce flat bunches with charges of 3.2 nC, 1.0 nC and 20 pC. The photocathode laser is taken to follow a Gaussian distribution with rms duration σ_t=3 ps. A uniform transverse laser intensity distribution was taken at the photocathode surface. An initial kinetic energy of 0.55 eV was used to simulate a thermal emittance contribution due to photoemission process from the Cs_2Te cathode.

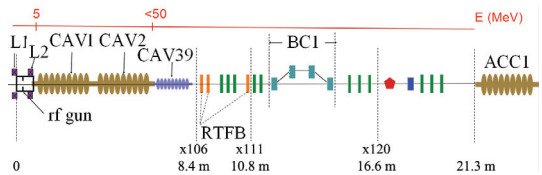

Figure 1: Overview of the ASTA photoinjector. R_{56} of BC1 is approximately 0.19 m.

The figure-of-merit $\varepsilon_{\text{FOM}}=\varepsilon_{\text{sub}}^2/2l$ was minimized at the location of the first skew quadrupole magnet by tuning the launch phase of the RF gun, the laser spot size, the peak fields of the main (L2) and bucking (L1) solenoidal lenses. The quantity ε_{sub} represent the uncorrelated transverse emittance computed in the Larmor's frame, e.g., after removal of the coupling between the two transverse phase spaces. Thus according to equation (1), ε_{FOM} should be close to $\varepsilon_{\text{eigen},-}$, as also observed in our simulations.

Once the optimized settings are obtained, the beam is transported through the RFBT. The strengths of the skew quadrupole magnets were determined as described in [7]. The resulting quadrupole-magnet strengths were then used in IMPACT-T [9] to track the beam evolution throughout the RFBT.

The optimized simulation results for various bunch charges are summarized in Table 1. The phase spaces for the optimized 3.2-nC flat beam appear in Fig. 2.

CHROMATIC ABERRATION

In order to compress the flat beam to produce a high peak current, a large longitudinal-phase-space (LPS) chirp is produced by off-crest acceleration in the booster cavity downstream of the photocathode. The chromatic aberration during the RFBT transformation will result in considerable emittance growth of the flat beam [10]. The relative flat-beam smaller-emittance growth during the RFBT is derived as:

$$\frac{\Delta\varepsilon_y}{\varepsilon_{y0}} \approx \frac{\left(\sum_{j=1}^{3} \left((1+\lambda_j) q_{0,j}^2 \left\langle x_{i,j}^2 \right\rangle \left\langle y_{i,j}^2 \right\rangle \right) - \varepsilon_{\text{eff}}^2 \right) \left\langle \delta^2 \right\rangle}{2\varepsilon_{y0}^2}, \quad (2)$$

where $q_{0,j}$ is the integral quadrupole strength of the j^{th} skew-quadrupole magnet, $x_{i,j}$ and $y_{i,j}$ are the coordinates of electrons at the entrance of the j^{th} skew-quadrupole

*Work supported by DOE Contracts No. DE-AC02-07CH11359 with the Fermi Research Alliance, LLC., No. DE-FG02-08ER41532 with the Northern Illinois University and fellowship from Battelle Memorial Institute.
#zhujun98@fnal.gov

ISBN: 978-3-95450-132-8 doi:10.18429/JACoW-IPAC2014-THPRO086

magnet, ε_{eff} is the geometric emittance of the magnetized beam upstream of the RFBT, ε_{y0} is the nominal vertical geometric emittance of the flat beam in absence of chromatic aberration and λ_j is coefficient with $0 \le \lambda_j \le 1$.

Table 1: Optimized Properties of the Flat Beams and Corresponding Injector Settings*

Bunch charge (nC)	3.2	1.0	0.02
Electron energy (MeV)	36.7	36.0	36.9
$\varepsilon_{n,x}$ (μm)	95.4	46.9	4.32
$\varepsilon_{n,y}$ (μm)	0.25	0.13	0.015
Laser spot size (mm)	1.26	0.93	0.25
Phase of gun (degree)	0.0	2.0	0.0
Peak field of main solenoid (T)	0.1468	0.1486	0.1400
Peak field of bucking solenoid (T)	0.1120	0.0972	0.1220
Peak field of CAV1 (MV/m)	27.0	25.0	24.0
Phase of CAV1 (degree)	-48.1	-47.3	-36.9

* The peak fields of the gun cavity and CAV2 are 40 and 42 MV/m respectively, and the CAV2 is operated on-crest.

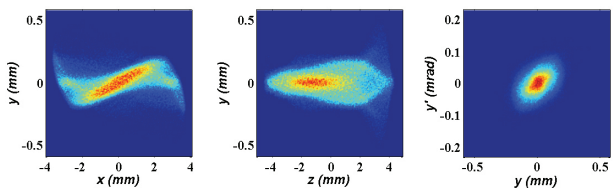

Figure 2: Configuration spaces (left, and middle) and vertical phase space (right) associated to a 3.2-nC flat beam.

As an example we consider the case of a 37-MeV 3.2-nC bunch; see Fig. 3 and 4. Here D_2 denotes the distance between the first two skew quadrupole magnets and D_T denotes the total length of the RFBT. Normally, the location of the second skew quadrupole magnet is been concerned for a RFBT with a given total length. The simulation results indicate that the first two skew-quadrupole magnets should be as close as possible. The rms. transverse beam sizes evolution along the RFBT beamline are shown in Fig. 5 for D_2/D_T=0.2 and 0.7 respectively. Since the vertical beam size at the third quadrupole magnet is extremely small, according to equation (2), the third quadrupole magnet will not significantly contribute to the emittance dilution caused by the chromatic aberration. When the distance between the first two skew quadrupole magnets increases, the transverse beam sizes at the second quadrupole magnet increase considerably. This increase results in a larger emittance growth. Note that the integral quadrupole strength of the second skew-quadrupole magnet is weakly dependent on the D_2/D_T ratio. Considering the case when D_2 is fixed, the integral quadrupole strengths of all the skew-quadrupole magnets decrease as D_T increases. This decrease in strength mitigates the emittance growth.

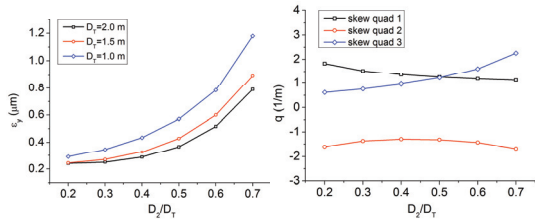

Figure 3: Vertical emittance of the 3.2-nC flat beam for different D_T (left) and corresponding integral quadrupole strengths for D_T=2.0 m (right), as a function of D_2/D_T.

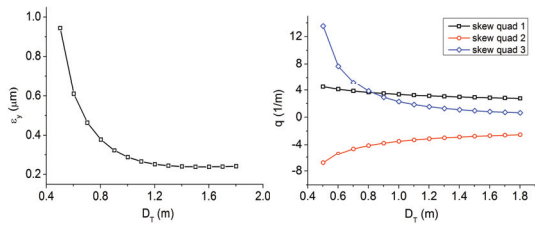

Figure 4: Vertical emittance of the 37-MeV, 3.2-nC flat beam with D_2=0.2 m (left) and the corresponding integral quadrupole strengths (right), as a function of D_T.

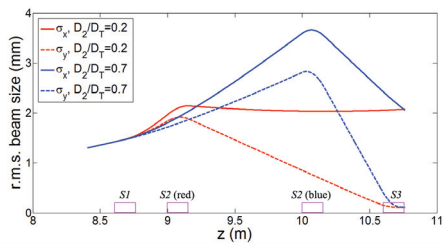

Figure 5: Transverse beam sizes evolution along the RFBT beamline for D_2/D_T=0.2 (red) and 0.7 (blue) with D_T=2 m. The S1, S2, S3 magenta rectangles indicate the location of the skew quadrupole magnets.

To convert a CAM-dominated beam into a flat beam, the following equation should be satisfied [5]

$$S = A_+^{-1} A_-, \tag{3}$$

where

$$S = \begin{bmatrix} \alpha & \beta \\ -\dfrac{1+\alpha^2}{\beta} & -\alpha \end{bmatrix}, \tag{4}$$

α, β are the Courant-Snyder parameters of the CAM-dominated beam, and $A_\pm$ are the 2×2 block matrices of the 4×4 transfer matrix of the RFBT. It is apparent that the left side of equation (3) is purely determined by the Courant-Snyder parameters of the initial CAM-dominated beam, while the right side of equation (3) is only determined by the RFBT settings. Since the energy spread of the beam before compression is dominated by the correlated energy spread, the chromatic effect could be compensated if a proper longitudinal correlation of the Courant-Snyder parameters could be added to the initial beam. The emittance compensation is demonstrated by

ISBN: 978-3-95450-132-8 doi:10.18429/JACoW-IPAC2014-THPRO086

our simulations, as shown in Fig. 6. When operating CAV1 (instead of CAV2) off-crest, the vertical emittance growth of the flat beam could be compensated to attain a value as low as the initial eigenemittance of the incoming CAM-dominated beam.

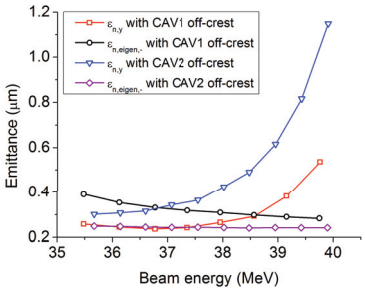

Figure 6: $\varepsilon_{n,eigen,-}$ (circle) and $\varepsilon_{n,y}$ (rectangular) with CAV1 operated off-crest, and $\varepsilon_{n,eigen,-}$ (diamond) and $\varepsilon_{n,y}$ (triangle) with CAV2 operated off-crest, as a function of beam energy for the 3.2-nC beam.

FLAT-BEAM COMPRESSION

To first order, the rms bunch length after the third dipole magnet is given as:

$$\sigma_{z_3} = \sqrt{\left(1 + hR_{56}^{(3)}\right)^2 \sigma_{z_0}^2 + R_{56}^{(3)2}\sigma_{\delta_u}^2 + E}\,, \qquad (5)$$

where

$$E = \frac{\varepsilon_x}{\beta_{x0}}\left(R_{52}^{(3)2} + (R_{52}^{(3)}\alpha_{x0} - R_{51}^{(3)}\beta_{x0})^2\right), \qquad (6)$$

$R_{51}^{(3)}$, $R_{52}^{(3)}$, $R_{56}^{(3)}$ are the elements of the transfer matrix from the entrance of the chicane to the exit of the third dipole magnet, ε_x is the geometric horizontal emittance of the beam, β_{x0}, α_{x0} are the horizontal Courant-Snyder parameters of the beam at the entrance of the chicane, $\sigma_{\delta u}$ is the r.m.s. uncorrelated fractional energy spread and σ_{z0} is the r.m.s. bunch length at the entrance of the chicane. It is found that equation (6) will dominate in the bunch length of the flat beam after the third dipole magnet. Therefore, the bunch can be de-compressed downstream the 3rd dipole magnet with proper optics.

The dynamics of the flat beam in BC1 was simulated with both ELEGANT [11] and IMPACT-T programs including CSR effect using the built-in 1-D model. The nominal optics and beam phases paces downstream of BC1 are shown in Fig. 7 and 8 respectively, and the relevant beam parameters of the compressed flat beam are summarized in Tab. 2. It is evident that the space charge effects play an important role in the compression of the low energy flat beam. Note that the vertical emittance growth shown by IMPACT-T simulation becomes notable only downstream BC1 because of the space charge force.

ACKNOWLEDGMENT

The authors would like to thank J. Qiang for providing us with a copy of the IMPACT-T code and for fruitful discussions. We are indebted to P. Czerpata, V. Shiltsev, E. Harms and R. Estrada for their support.

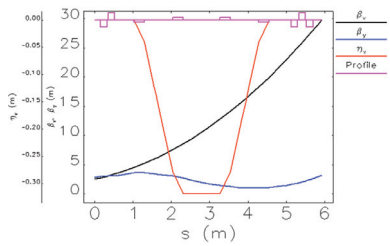

Figure 7: Nominal lattice functions along the BC1 chicane.

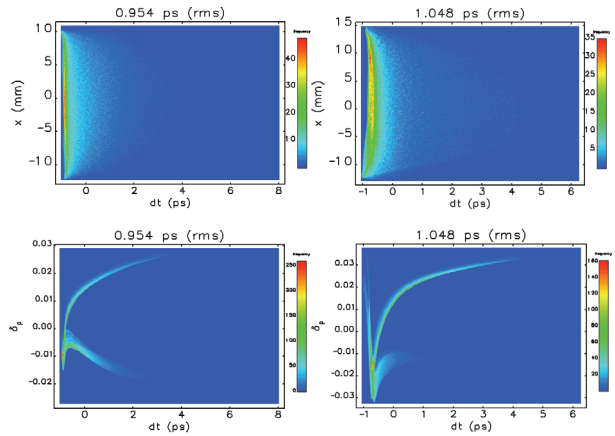

Figure 8: Beam phase space downstream of BC1 simulated using ELEGANT (left row) and simulated using IMPACT-T (right row). The initial phasespace was simulated using IMPACT-T with 400 k macroparticles.

Table 2: Properties of the Compressed 3.2-nC Flat Beam

Simulation program	ELEGANT	IMPACT-T
Energy loss (MeV)	0.37	0.64
$\Delta\varepsilon_{n,x}/\varepsilon_{n,x}$ (%)	4.3%	15.9%
$\Delta\varepsilon_{n,y}/\varepsilon_{n,y}$ (%)	0	45.8%
Peak current (kA)	5.2	5.5

REFERENCES

[1] R. Brinkmann et al., Phys. Rev. ST Accel. Beams 4, 053501 (2001).
[2] K.-J. Kim et al., Phys. Rev. ST Accel. Beams 10, 080702 (2007).
[3] D. Mihalcea et al., Phys. Rev ST Accel. Beams 15, 081304 (2012).
[4] A. Valloni et al., AIP Conf. Proc. 1507, 762 (2012 Austin AAC)
[5] K.-J. Kim, Phys. Rev. ST Accel. Beams 6, 104002 (2003).
[6] A. Dragt et al., Phys. Rev. A 45, 2572 (1992)
[7] P. Piot et al., Phys. Rev. ST Accel. Beams 9, 031001 (2006).
[8] K. Flöttmann, ASTRA particle tracking code http://www.desy. de/ ~mpyflo/
[9] J. Qiang, S. Lidia, R. D. Ryne, C. Limborg-Deprey, Phys. Rev. ST Accel. Beams, 9 (2006) 044204.
[10] Y.-E Sun et al., in proceedings of LINAC 2004, Lübeck, Germany, 2004, p. 150.
[11] M. Borland, Phys. Rev. ST Accel. Beams 4, 070701 (2001).